A numerical scheme for two-scale phase-field models in porous media

Manuela Bastidas*, Sohely Sharmin*, Carina Bringedal† and Sorin Pop*

* Faculty of Sciences
Hasselt University
Diepenbeek, Belgium
e-mail: manuela.bastidas@uhasselt.be, sohely.sharmin@uhasselt.be, sorin.pop@uhasselt.be

† Institute for Modelling Hydraulic and Environmental Systems,
University of Stuttgart
Stuttgart, Germany
e-mail: carina.bringedal@iws.uni-stuttgart.de

Key words: Multi-scale methods, phase-field models, two-phase flow

Abstract: *We consider the flow of two immiscible fluid phases in a porous medium. At the scale of pores, the two fluid phases are separated by interfaces that are transported by the flow. Furthermore, the surface tension at such interfaces depends on the concentration of a surfactant dissolved in one of the fluids. Here we discuss a two-scale model for two-phase porous-media flow, in which concentration-dependent surface tension effects are incorporated. The model is obtained by employing formal homogenization methods and relies on the phase-field approach, in which thin, diffuse interface regions approximate the interfaces. We propose a two-scale numerical scheme and present numerical results revealing the influence of various quantities on the averaged behaviour of the system.*

1 INTRODUCTION

Porous media are complex domains involving many alternating solid grains surrounded by void spaces (the pores). These form hierarchically organized structures in which various processes take place at different scales. Prominent examples in this sense are the fluid flow through the pores of the medium, the transport of chemically reactive substances, or mechanical deformation. In situations like the ones mentioned here, there are processes taking place at the scale of pores (from now on called the micro scale), whereas the main interest is in the averaged behavior of the system at a larger scale (the laboratory or even the field scale, from now on called the macro scale).

Two-phase flow in porous media are encountered in several real-life situations of practical relevance. Prominent examples in this sense are geological CO2 sequestration or oil recovery. Here we consider the flow of two immiscible fluid phases in a porous medium. At the micro scale, one encounters an interface separating the two fluids transported by the flow. Furthermore, we assume that the surface tension may change depending on the concentration of a surfactant dissolved in one of the fluid phases. Since the location of the interface is not known a-priori but depends on the (unknown) fluid velocities and the surfactant concentration, the resulting mathematical model involves free boundaries at the micro scale. Hence, the model equations are defined in time-dependent a-priori unknown micro-scale domains.

Two significant challenges can be identified in this context: the free boundaries at the micro scale and the complex structure of the micro-scale domain. To deal with the former, we consider a phase-field approach, in which the evolving interfaces are approximated by narrow diffuse-interface regions, which allows defining all model components on the entire micro-scale domain. For the latter, we recall that in practical applications, the main interest is in the system's behavior at the macro scale, not necessarily in the complex, micro-scale behavior.

https://doi.org/10.4995/YIC2021.2021.12571

Therefore, we apply formal homogenization techniques to derive a two-scale phase-field model, approximating the averaged, macro-scale behavior of the system. In the resulting two-scale model, the effective (macro-scale) parameters required at the macro scale are determined by solving micro-scale cell problems, which, in their turn, depend on the macro-scale quantities.

Similar situations are considered in [1,2], where macro-scale models are derived for two-phase porous-media flow, accounting for the evolving interfaces at the micro scale. Such results are extended in [3], where dynamic and hysteretic contact angles are incorporated in the micro-scale model before deriving macro-scale ones. Closest to the present contribution is the case involving a concentration-dependent surface tension studied in [4]. However, all these results are obtained for sharp-interface micro-scale models.

Phase-field models for two-phase porous-media flow, including the derivation of macro-scale models are discussed in [5–10]. More precisely, in [5, 6] phase-field pore-scale models are discussed, and the convergence to the corresponding sharp-interface model is proved when passing the diffuse-interface parameter to zero. A macro-scale model is derived in [9] under certain scaling assumptions, but without accounting for variable surface-tension effects. A macro-scale phase-field model for compressible fluids is derived in [8]. Here we consider a two-scale phase-field model derived by formal homogenization techniques [11]. The model includes variable surface-tension effects, depending on the concentration of a surfactant dissolved in one of the fluid phases. We propose an explicit numerical scheme, accounting for the coupling between the two scales.

The paper is organized as follows. In Section 2, the two-scale model is presented, and the interaction between the scales is highlighted. Then, in Section 3, an explicit numerical scheme is proposed for the numerical solution of the two-scale model. Finally, in Section 4, a numerical example is presented, for which the necessity of using adaptive meshes at the micro scale is discussed, and the influence of the macro-scale quantities on the micro-scale results is studied.

2 THE TWO-SCALE MODEL

At the macro scale, the porous medium is a bounded domain $\Omega \subset \mathbb{R}^2$, having Lipschitz-continuous boundary $\partial\Omega$. Let $\mathrm{T} \in (0, \infty)$ be the final time. To each macro-scale point $\mathbf{x} \in \Omega$, one micro-scale cell $Y = [0, 1]^2$ is associated. The micro-scale cell is divided into two subdomains: the inner grain G surrounded by the pore space P. We denote by ∂G the boundary of G and by $\mathbf{n}$ the unit normal to ∂G pointing into G. One has $Y = G \cup P \cup \partial G$, and we assume that the pore space P is filled by two fluids, "Fluid 1" and "Fluid 2". A sketch of the two-scale domain is shown in Figure 1.

Following the phase-field approach, the (micro-scale) sharp interface separating the two fluids is replaced by a narrow, diffuse interface. Consequently, the two fluids are identified at the micro scale through the phase field ϕ, ranging from 1 (corresponding to Fluid 1) to -1 (for Fluid 2). At the micro scale, this allows defining the velocity, pressure, and solute concentration for the mixture over the entire pore space P, without separating between the fluid phases. The corresponding macro-scale quantities are $\bar{\mathbf{v}}$, $\bar{\mathbf{v}}_\phi$, p and c. Also, S stands for the macro-scale saturation of Fluid 1. We consider the following macro-scale model for $\mathbf{x} \in \Omega$ and $t \in (0, T]$

$$(\mathbf{P}_p) \qquad \begin{cases} \bar{\mathbf{v}} = -\mathcal{K}\nabla p - \mathbf{M}\gamma(c), \\ \nabla \cdot \bar{\mathbf{v}} = 0, \end{cases}$$

$$(\mathbf{P}_S) \qquad \begin{cases} \bar{\mathbf{v}}_\phi = -\mathcal{K}_\phi \, \nabla p - \mathbf{M}_\phi \, \gamma(c), \\ \Phi \, \partial_t S + \dfrac{1}{2} \nabla \cdot \bar{\mathbf{v}}_\phi = 0, \end{cases}$$

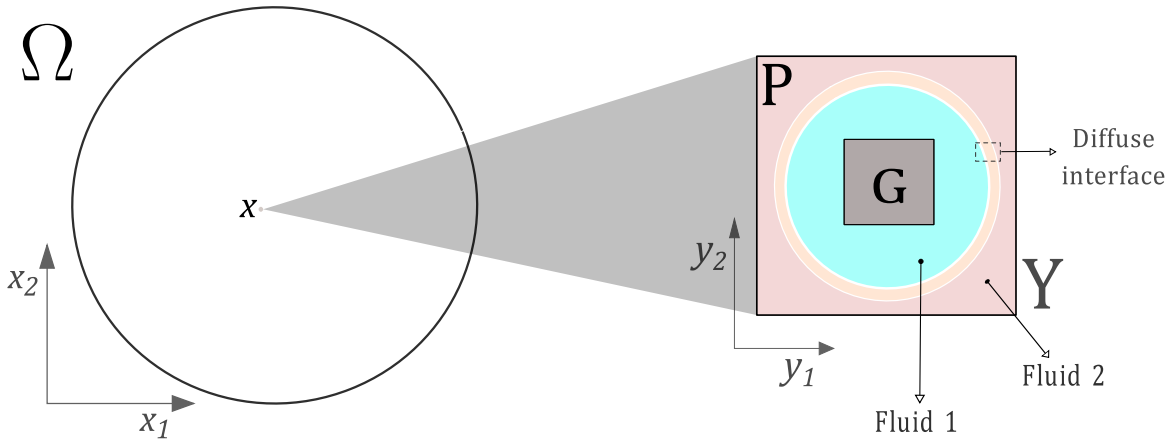

Figure 1: The porous medium: the macro-scale domain Ω (left) and the micro-scale domain Y (right) corresponding to a point $\mathbf{x} \in \Omega$.

$$(\mathbf{P}_c) \qquad \Phi\, \partial_t(Sc) + \frac{1}{2}\nabla \cdot (c(\bar{\mathbf{v}} + \bar{\mathbf{v}}_\phi)) = \frac{1}{\overline{\mathrm{Pe}_c}}\nabla \cdot (\mathcal{B}\nabla c + \mathbf{H}c).$$

Initial and boundary conditions complete the model. Here $\overline{\mathrm{Pe}_c}$ is the non-dimensional Péclet number and Φ denotes the medium porosity. The definition of the effective parameters $\mathcal{K}_\phi$, $\mathcal{K}$, $\mathbf{M}_\phi$, $\mathbf{M}$, $\mathcal{B}$, $\mathbf{H}$ depend on the micro-scale structure and on the evolution of the micro-scale phase field ϕ, as explained below. Note that $\bar{\mathbf{v}}$ is the velocity of the mixture of the two fluids, while $\bar{\mathbf{v}}_\phi$ accounts for the phase distribution. Hence $\frac{1}{2}(\bar{\mathbf{v}} + \bar{\mathbf{v}}_\phi)$ reflects the macro-scale velocity of Fluid 1.

At each micro-scale cell Y, the phase field ϕ and the potential ψ are computed by solving the following micro-scale cell problem

$$(\mathbf{P}_\phi) \qquad \begin{cases} \nabla \cdot (\mathbf{v}\phi) = \overline{\mathrm{A}_\phi}\lambda\Delta\psi, & \text{in } P, \\ \psi = \dfrac{\overline{\mathrm{A}_\psi}\gamma(c)}{\lambda}\left(\mathcal{C}P'(\phi) + I'(\phi) - \mathcal{C}\lambda^2\Delta\phi\right), & \text{in } P, \\ \nabla\phi \cdot \mathbf{n} = 0, & \text{on } \partial G, \\ \nabla\psi \cdot \mathbf{n} = 0, & \text{on } \partial G, \\ \phi,\ \psi \text{ are } Y\text{-periodic}, \\ \dfrac{1}{\Phi}\displaystyle\int_P \phi\, d\mathbf{y} = (2S - 1)\,. \end{cases}$$

Observe that t enters in $(\mathbf{P}_\phi)$ as a parameter, through the macro-scale saturation S and concentration c. Here $\overline{\mathrm{A}_\phi}, \overline{\mathrm{A}_\psi}$ are non-dimensional quantities and $\gamma(c)$ is the concentration-dependent surface tension, which introduces a coupling with the macro scale. The micro-scale velocity $\mathbf{v}$ is defined below and its average is by construction $\bar{\mathbf{v}}$. Moreover, we choose $P(\phi) = \frac{1}{4}(1-\phi^2)^2$ as the double-well type potential and $I(\phi) = \frac{1}{2}(1+\phi)$ as a characteristic function which is 1 in Fluid 1 and 0 in Fluid 2. The parameter λ is the diffuse interface thickness and $\mathcal{C} = \frac{3}{2\sqrt{2}}$ is a calibration constant.

The components of the effective matrices $\mathcal{K}$ and $\mathcal{K}_\phi$, appearing in the Darcy-type laws in $(\mathbf{P}_p)$ and in the evolution equation for the saturation $(\mathbf{P}_S)$, are found through

$$\mathcal{K}_{\mathtt{s},\mathtt{r}} = \int_P (\mathbf{w}_\mathtt{r})_\mathtt{s}\, d\mathbf{y} \quad \text{and} \quad (\mathcal{K}_\phi)_{\mathtt{s},\mathtt{r}} = \int_P (\mathbf{w}_\mathtt{r})_\mathtt{s}\phi\, d\mathbf{y}, \qquad \text{for } \mathtt{r},\mathtt{s} = 1,2. \tag{1}$$

Here $(\mathbf{w}_\mathtt{r})_\mathtt{s}$ are the components of $\mathbf{w}_\mathtt{r} = ((\mathbf{w}_\mathtt{r})_1, (\mathbf{w}_\mathtt{r})_2)^t$, where $(\mathbf{w}_\mathtt{r}, \Pi_\mathtt{r})$ solve the following

Stokes-type cell problems

$$(\mathbf{P}^{\mathtt{r}}_{\mathcal{K}}) \qquad \begin{cases} \overline{\mathrm{Eu}}\,(\mathbf{e}_{\mathtt{r}} + \nabla\Pi_{\mathtt{r}}) = -\dfrac{1}{\overline{\mathrm{Re}}}\nabla\cdot(2\mu(\phi)\boldsymbol{\varepsilon}(\mathbf{w}_{\mathtt{r}}))\,, & \text{in } P,\\ \nabla\cdot\mathbf{w}_{\mathtt{r}} = 0, & \text{in } P,\\ \mathbf{w}_{\mathtt{r}} = \mathbf{0}, & \text{on } \partial G,\\ \Pi_{\mathtt{r}}, \mathbf{w}_{\mathtt{r}} \text{ are } Y\text{-periodic} \quad \text{and} \quad \displaystyle\int_P \Pi_{\mathtt{r}}\, d\mathbf{y} = 0. \end{cases}$$

Here $\boldsymbol{\varepsilon}(\mathbf{w}_{\mathtt{r}}) = \frac{1}{2}\left((\nabla\mathbf{w}_{\mathtt{r}}) + (\nabla\mathbf{w}_{\mathtt{r}})^T\right)$ is the symmetric stress tensor and $\mathbf{e}_{\mathtt{r}}$ is the unit basis vector. The Euler and Reynolds numbers are denoted by $\overline{\mathrm{Eu}}$ and $\overline{\mathrm{Re}}$, respectively. Moreover, $\mu(\phi) = \frac{\mu^2\cdot(1+\phi)}{2} + \frac{\mu^1\cdot(1-\phi)}{2}$ is the viscosity of the mixture of the two fluids and μ^i with $i = 1, 2$ correspond to the viscosity of Fluid i. As before, t enters in $(\mathbf{P}^{\mathtt{r}}_{\mathcal{K}})$ as a parameter through ϕ.

Additionally, the components of the effective vectors $\mathbf{M}$ and $\mathbf{M}_\phi$, appearing in the Darcy-type law $(\mathbf{P}_p)$ and in the evolution equation for the saturation $(\mathbf{P}_S)$, are found through

$$\mathbf{M}_{\mathtt{s}} = \int_P (\mathbf{w}_0)_{\mathtt{s}}\, d\mathbf{y} \quad \text{and} \quad (\mathbf{M}_\phi)_{\mathtt{s}} = \int_P (\mathbf{w}_0)_{\mathtt{s}}\phi\, d\mathbf{y}, \qquad \text{for } \mathtt{r}, \mathtt{s} = 1, 2. \tag{2}$$

As before, $(\mathbf{w}_0)_{\mathtt{s}}$ are the components of $\mathbf{w}_0 = ((\mathbf{w}_0)_1, (\mathbf{w}_0)_2)^t$, where $(\mathbf{w}_0, \Pi_0)$ solve the following modified Stokes-type cell problem

$$(\mathbf{P}_{\mathbf{M}}) \qquad \begin{cases} \overline{\mathrm{Eu}}\nabla\Pi_0 = -\dfrac{1}{\overline{\mathrm{Re}}}\nabla\cdot(2\mu(\phi)\boldsymbol{\varepsilon}(\mathbf{w}_0)) + \dfrac{\mathcal{C}}{\overline{\mathrm{Re}}\;\overline{\mathrm{Ca}}}\left(\dfrac{1}{\lambda}P'(\phi) - \lambda\Delta\phi\right)\nabla\phi, & \text{in } P,\\ \nabla\cdot\mathbf{w}_0 = 0, & \text{in } P,\\ \mathbf{w}_0 = \mathbf{0}, & \text{on } \partial G,\\ \Pi_0, \mathbf{w}_0 \text{ are } Y\text{-periodic} \quad \text{and} \quad \displaystyle\int_P \Pi_0\, d\mathbf{y} = 0, \end{cases}$$

with $\overline{\mathrm{Ca}}$ being the capillary number. Observe that $(\mathbf{P}_{\mathbf{M}})$ is introduced to deal with the concentration-dependent surface tension.

The micro-scale cell velocities $\mathbf{w}_{\mathtt{r}}$ and $\mathbf{w}_0$ are also involved in the calculation of the micro-scale velocity $\mathbf{v}$, i.e.

$$\mathbf{v} = -\sum_{\mathtt{r}=1}^{2} \mathbf{w}_{\mathtt{r}}\, \partial_{x_{\mathtt{r}}} p - \mathbf{w}_0\gamma(c). \tag{3}$$

Notice that the macro-scale velocities $\bar{\mathbf{v}}$ and $\bar{\mathbf{v}}_\phi$ in $(\mathbf{P}_p)$ are related with the micro scale trough $\mathbf{v}$ and ϕ as follows

$$\bar{\mathbf{v}} = \int_P \mathbf{v}\, d\mathbf{y} \quad \text{and} \quad \bar{\mathbf{v}}_\phi = \int_P \mathbf{v}\phi\, d\mathbf{y}.$$

The components of the effective matrix $\mathcal{B}$ and the effective vector $\mathbf{H}$, appearing in the macro-scale equation for the solute concentration $(\mathbf{P}_c)$, are

$$\mathcal{B}_{\mathtt{s},\mathtt{r}} = \int_P I(\phi)\,(\delta_{\mathtt{s},\mathtt{r}} + \partial_{y_{\mathtt{s}}}\chi_{\mathtt{r}})\; d\mathbf{y}, \quad \mathbf{H}_{\mathtt{s}} = \int_P I(\phi)\partial_{y_{\mathtt{s}}}\chi_0\, d\mathbf{y}, \qquad \text{for } \mathtt{r}, \mathtt{s} = 1, 2. \tag{4}$$

Here, $\chi_{\mathtt{r}}$ and χ_0 solve the following micro-scale cell problems

$$(\mathbf{P}^{\mathtt{r}}_{\mathcal{B}}) \qquad \begin{cases} \nabla\cdot[I(\phi)\,(\nabla\chi_{\mathtt{r}} + \mathbf{e}_{\mathtt{r}})] = 0, & \text{in } P,\\ I(\phi)\,(\nabla\chi_{\mathtt{r}} + \mathbf{e}_{\mathtt{r}})\cdot\mathbf{n} = 0, & \text{on } \partial G,\\ \chi_{\mathtt{r}} \text{ is } Y\text{-periodic} \quad \text{and} \quad \displaystyle\int_P \chi_{\mathtt{r}}\, d\mathbf{y} = 0. \end{cases}$$

$$(\mathbf{P_H}) \qquad \begin{cases} \nabla \cdot [I(\phi)\nabla\chi_0] = \nabla \cdot (I(\phi)\mathbf{v}), & \text{in } P, \\ I(\phi)\nabla\chi_0 \cdot \mathbf{n} = 0, & \text{on } \partial G, \\ \chi_0 \text{ is } Y\text{-periodic} \quad \text{and} \quad \displaystyle\int_P \chi_0 \, d\mathbf{y} = 0. \end{cases}$$

3 THE NUMERICAL SCHEME

We propose an explicit numerical scheme for solving the two-scale model for the two-phase flow porous-media problem presented in Section 2. With $N \in \mathbb{N}$, we let $\Delta t = \mathrm{T}/N$ be the time step size and define $t^n = n\Delta t$. The time-discrete solutions are denoted by $\phi^n := \phi(\cdot, \cdot, t^n)$ and $\nu^n := \nu(\cdot, t^n)$ where $\nu \in \{\mathcal{K}_\phi, \mathcal{K}, \mathbf{M}_\phi, \mathbf{M}, \mathcal{B}, \mathbf{H}, p, \bar{\mathbf{v}}, \bar{\mathbf{v}}_\phi, S, c\}$. For $n \geq 0$, assume S^n, c^n and ϕ^n given. The time stepping reads:

- For each $\mathbf{x} \in \Omega$, compute the solution of the time-discrete micro-scale cell problems corresponding to $(\mathbf{P}^{\mathrm{r}}_{\mathcal{K}})$ and $(\mathbf{P_M})$.
- Compute the first set of time-discrete effective parameters $\mathcal{K}^n_\phi$, $\mathcal{K}^n$, $\mathbf{M}^n_\phi$ and $\mathbf{M}^n$.
- Compute the macro-scale solution p^n and $\bar{\mathbf{v}}^n$ by solving the time-discrete macro-scale problems corresponding to $(\mathbf{P}_p)$.
- Compute the macro-scale solution $\bar{\mathbf{v}}^n_\phi$ and S^{n+1} by solving the time-discrete macro-scale problems corresponding to $(\mathbf{P}_S)$.
- For each $\mathbf{x} \in \Omega$, compute the micro-scale velocity $\mathbf{v}^n$ and the solution of the time-discrete micro-scale cell problems corresponding to $(\mathbf{P}^{\mathrm{r}}_{\mathcal{B}})$ and $(\mathbf{P_H})$.
- Compute the second set of time-discrete effective parameters $\mathcal{B}^n$ and $\mathbf{H}^n$.
- Compute the macro-scale solution c^{n+1} by solving the time discrete problem corresponding to $(\mathbf{P}_c)$.
- For each $\mathbf{x} \in \Omega$, compute the solution of the time-discrete phase-field problem corresponding to $(\mathbf{P}_\phi)$ to obtain ϕ^{n+1}.

The explicit scheme is sketched in Figure 2. We highlight that the two-scale problem itself is fully coupled, and an iterative structure could be considered here. We refer to [12,13] for similar approaches using iterations to handle the multi-scale interaction between the sub-problems.

Clearly, for the numerical simulations the explicit time stepping needs to be completed by the spatial discretization. More precisely, let $\mathfrak{T}_H$ be a triangular partition of the macro-scale domain Ω with elements T of diameter H_T and $H := \max_{T \in \mathfrak{T}_H} H_T$. For computing the micro-scale quantities, a micro-scale domain Y is assigned to each macro-scale element T. On each micro-scale domain Y we define another triangular partition $\mathfrak{T}_h$ with elements T_μ of diameter h_{T_μ} and $h := \max_{T_\mu \in \mathfrak{T}_h} h_{T_\mu}$. Finally, we use the mixed finite element method to calculate the numerical solution at both scales. For an effective computation we use adaptive mesh refinement on the micro scale (see [12, 14]).

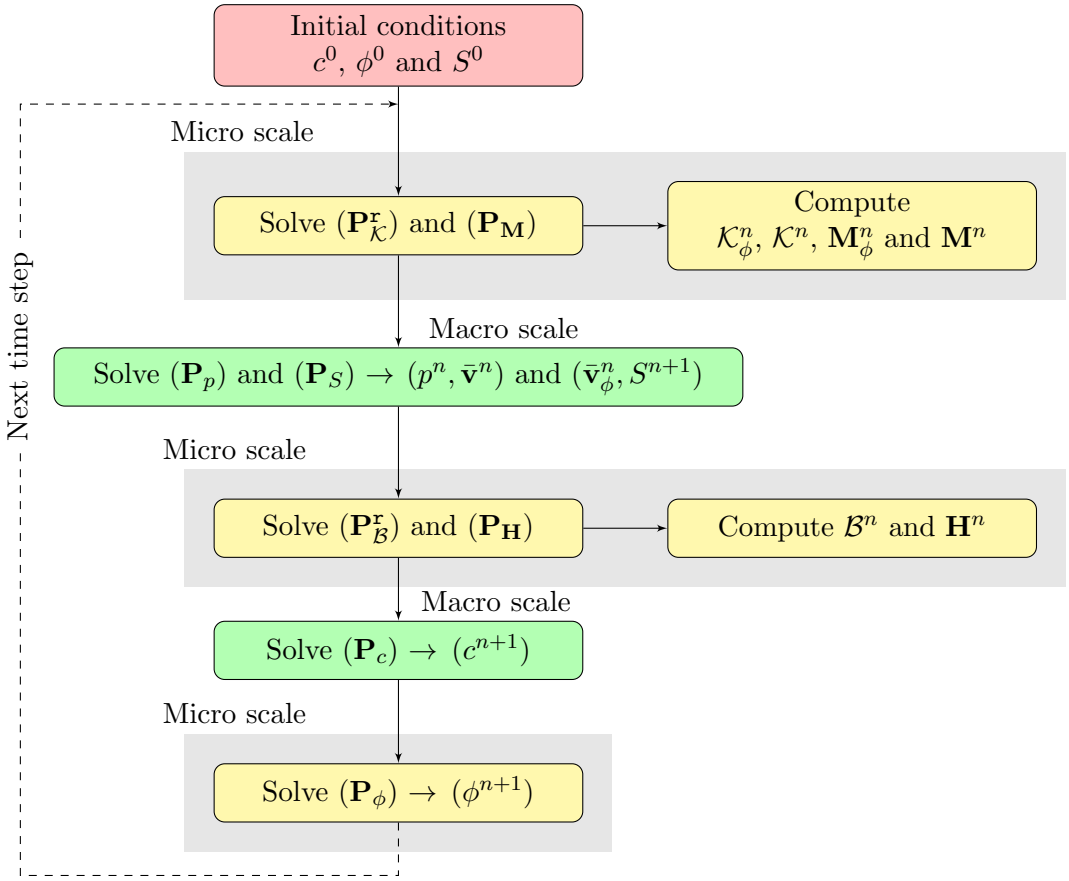

Figure 2: The explicit two-scale scheme.

4 NUMERICAL RESULTS

In this section, we present a micro-scale numerical experiment that highlights the relation between the macro-scale quantities and the micro-scale solutions. We restrict our implementations to the 2D case and all parameters remain non-dimensional. Here the micro-scale domain contains a centered square grain with side lengths 0.2 and we choose

$$\overline{\mathrm{Pe}_c} = \overline{\mathrm{Eu}} = \overline{\mathrm{Re}} = \overline{\mathrm{Ca}} = \overline{\mathrm{A}_\phi} = \overline{\mathrm{A}_\psi} = 1 \ \text{ and } \ \lambda = 0.08.$$

4.1 THE PHASE-FIELD AND THE MICRO-SCALE MESH

Figure 3 shows the initial phase field ϕ, corresponding to a saturation $S^0 = 0.639$, and the Laplacian of the initial phase field $\Delta\phi$, which is needed for computing the potential ψ in $(\mathbf{P}_\phi)$. The Laplacian is calculated numerically, and this calculation requires the construction of a very fine mesh around the transition zone to achieve sufficient accuracy. Close to the diffuse interface, the resolution of the micro-scale mesh $\mathfrak{T}_h$ is taken $h \ll \lambda$ to capture the diffuse transition zone and the variation in its derivatives. Following the ideas in [12], we refine the micro-scale mesh only close to the diffuse transition zone, making the computation of the phase field and the effective parameters accurate and efficient.

In Figure 3 we use an initially uniform mesh with 800 elements. Then, the mesh is refined around the transition zone such that the length of the smallest edge in the mesh is $\min_{T_\mu \in \mathfrak{T}_h} h_{T_\mu} = 1.25\text{E-}2 < \lambda$ and the length of the largest edge (located far from the transition zone) is $\max_{T_\mu \in \mathfrak{T}_h} h_{T_\mu} = 7.071\text{E-}2$.

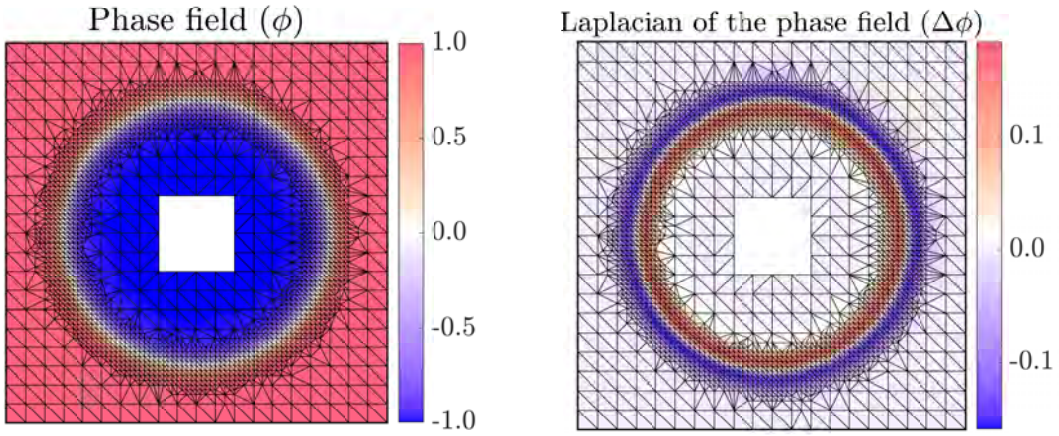

Figure 3: Phase-field initial condition (left) and the numerical calculation of the Laplacian of the phase field (right).

4.2 FIRST SET OF MICRO-SCALE PROBLEMS

Given the phase-field initial condition in Figure 3, we solve the micro-scale problems $(\mathbf{P}^{\mathbf{r}}_{\mathcal{K}})$ and $(\mathbf{P}_{\mathbf{M}})$ over the refined mesh. Figure 4 shows the scalar solutions Π_1, Π_2 and Π_0 of the problems $(\mathbf{P}^{\mathbf{r}}_{\mathcal{K}})$ and $(\mathbf{P}_{\mathbf{M}})$ in the simple case when the two fluids have the same viscosity, i.e. $\mu^1 = 1$ and $\mu^2 = 1$.

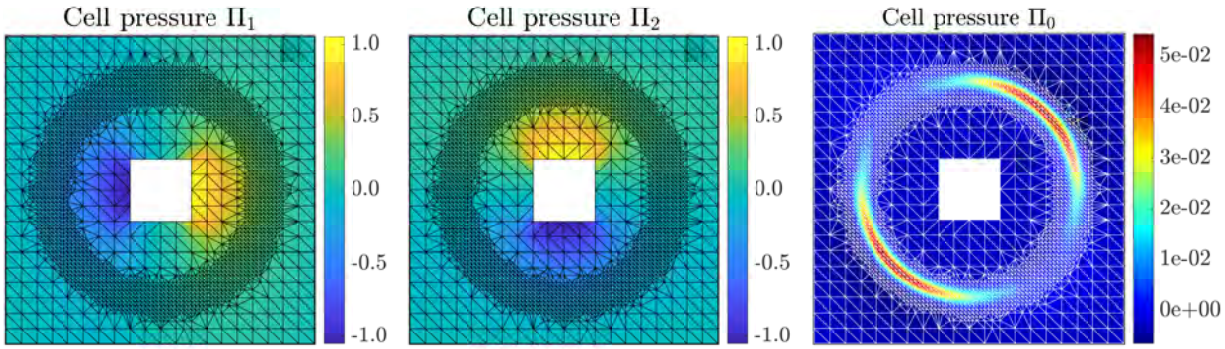

Figure 4: The solution of the first set of micro-scale problems $(\mathbf{P}^{\mathbf{r}}_{\mathcal{K}})$ (left and middle) and $(\mathbf{P}_{\mathbf{M}})$ (right).

Notice that for Π_0, the location of the changes in the solution coincides with the phase-field transition zone. This supports the requirement of a mesh refinement strategy to improve the accuracy and efficiency of further computations.

4.3 THE EFFECTIVE PARAMETERS

We show below the behavior of the effective parameters $\mathcal{K}_\phi$, $\mathcal{K}$, $\mathbf{M}_\phi$ and $\mathbf{M}$, depending on the saturation. Figure 5 displays the results for the effective tensors $\mathcal{K}_\phi$ and $\mathcal{K}$. We consider two cases: a simple case where the two fluids have same viscosity, i.e. $\mu^1 = \mu^2 = 1$, and a more complex case where the viscosities are $\mu^1 = 0.1$ and $\mu^2 = 1$.

The symmetry of the phase field at the micro scale implies that the effective tensors are isotropic. The non-diagonal components of $\mathcal{K}_\phi$ and $\mathcal{K}$ can be neglected, and in Figure 5 we only show the first component of the effective tensors.

Notice that when $\mu^1 = \mu^2 = 1$, the changes on the saturation do not affect the permeability $\mathcal{K}$. This is expected since the two fluids flow like one. In contrast, Figure 5 reflects that the changes in the saturation have an important effect if the two fluids have different viscosities.

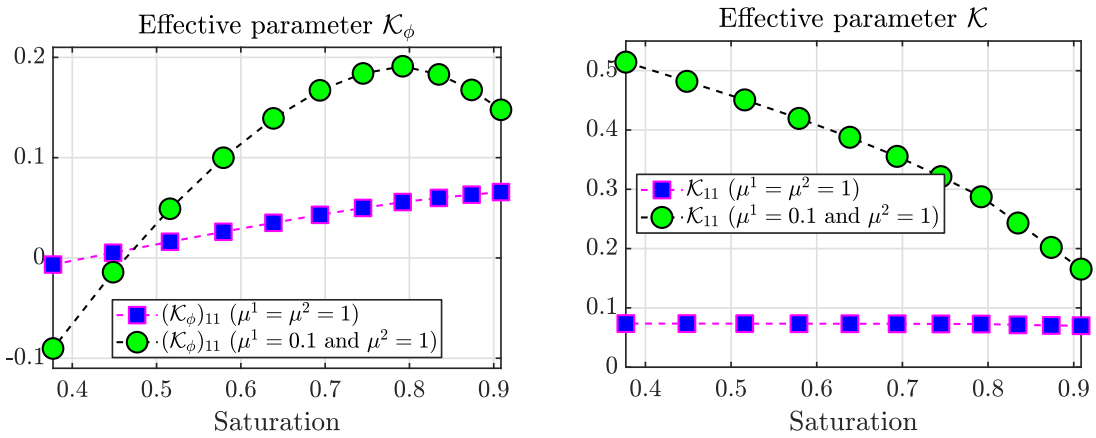

Figure 5: Dependence of the effective parameters $\mathcal{K}_\phi$ and $\mathcal{K}$ on the macro-scale saturation.

Commonly used two-phase porous-media flow models are relying on saturation-dependent quantities like relative permeability and capillary pressure. The situation here is similar, but capillary pressure is absent due to the assumed scaling of the capillary number [11]. Moreover, here $\mathcal{K}$ is not separated into absolute and relative permeability, and it reflects how the velocity of the mixture of the two fluids relate to the pressure gradient.

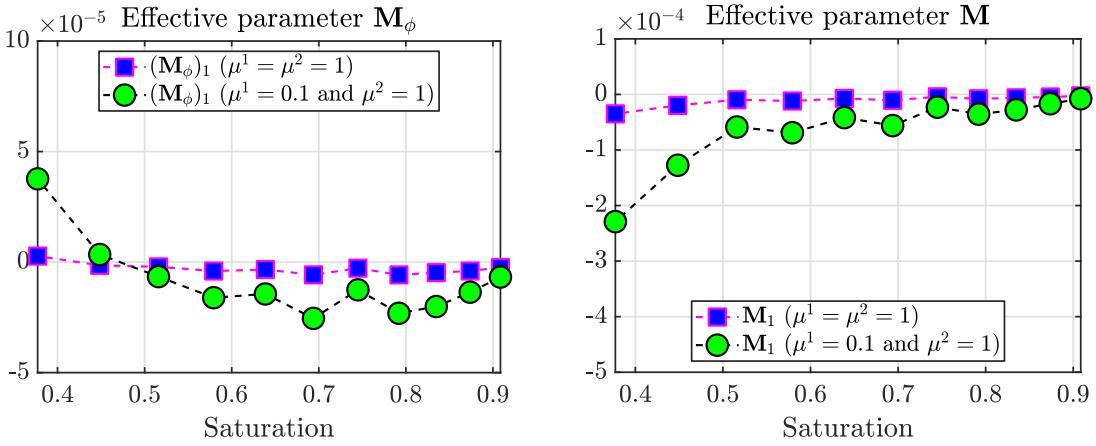

Figure 6: Dependence of the effective parameters $\mathbf{M}_\phi$ and $\mathbf{M}$ on the macro-scale saturation.

In Figure 6 we denote by $(\mathbf{M}_\phi)_1$ and $\mathbf{M}_1$ the first component of the effective vectors $\mathbf{M}_\phi$ and $\mathbf{M}$. Notice that for these macro-scale vectors, both components are equal due to the symmetry of the phase field. Moreover, Figure 6 shows that the variations in the effective parameters $\mathbf{M}_\phi$ and $\mathbf{M}$ are more relevant in the case of a large viscosity ratio.

5 SUMMARY AND OUTLOOK

We have considered a two-scale model for two-phase flow in a porous medium. The model describes the behavior of the mixture of two fluids and a surfactant dissolved into one of them. Here, the surface tension depends on the concentration of the solute. This model is the homogenized counterpart of a pore-scale phase-field model. For these phase-field formulations, a diffuse region approximates the moving interfaces separating the two fluids.

Based on the Euler explicit time stepping and the lowest order mixed finite element spatial discretization, we have proposed a two-scale numerical scheme. The scheme requires solving several micro-scale cell problems for each macro-scale point, depending on the macro-scale concentration and saturation. The solution of these micro-scale cell problems is used to deter-

mine the macro-scale parameters needed to compute the macro-scale model unknowns (velocity, pressure, saturation and concentration). For each micro-scale cell problem, the spatial mesh is refined or coarsened adaptively, improving the efficiency of the scheme.

We have presented numerical simulation results in two different situations, when the fluids have the same viscosities or when the viscosity ratio is large. Based on these results, we show the dependence of the macro-scale parameters depending on the saturation.

In the following research steps, we will analyze the possibility to compute the macro-scale parameters adaptively based on an active-passive node strategy. Furthermore, implicit or semi-implicit schemes will be considered, coupled with appropriate linearization approaches. Also, different regimes will be analyzed, possibly leading to models involving a capillary pressure.

ACKNOWLEDGEMENTS

This research is supported by the Research Foundation - Flanders (FWO) through the Odysseus programme (Project G0G1316N) and by the German Research Foundation (DFG) through the SFB 1313, Project Number 327154368.

REFERENCES

[1] A. Mikelic and L. Paoli, "On the derivation of the Buckley-Leverett model from the two fluid Navier-Stokes equations in a thin domain," *Computational Geosciences*, vol. 4, no. 1, pp. 99–101, 2000.

[2] D. Picchi and I. Battiato, "The impact of pore-scale flow regimes on upscaling of immiscible two-phase flow in porous media," *Water resources research*, vol. 54, no. 9, pp. 6683–6707, 2018.

[3] S. B. Lunowa, C. Bringedal, and I. S. Pop, "On an averaged model for immiscible two-phase flow with surface tension and dynamic contact angle in a thin strip," *Studies in Applied Mathematics*, vol. 1, p. 43, 2021.

[4] S. Sharmin, C. Bringedal, and I. S. Pop, "On upscaling pore-scale models for two-phase flow with evolving interfaces," *Advances in Water Resources*, vol. 142, p. 103646, 2020.

[5] H. Abels, H. Garcke, and G. Grün, "Thermodynamically consistent, frame indifferent diffuse interface models for incompressible two-phase flows with different densities," *Mathematical Models and Methods in Applied Sciences*, vol. 22, no. 03, pp. 1 150 013, 40, 2012.

[6] H. Garcke, K. F. Lam, and B. Stinner, "Diffuse interface modelling of soluble surfactants in two-phase flow," *Communications in Mathematical Sciences*, vol. 12, no. 8, pp. 1475–1522, 2014.

[7] O. R. A. Dunbar, K. F. Lam, and B. Stinner, "Phase field modelling of surfactants in multi-phase flow," *Interfaces and Free Boundaries*, vol. 21, no. 4, pp. 495–547, 2019.

[8] C. Rohde and L. von Wolff, "Homogenization of Nonlocal Navier–Stokes–Korteweg Equations for Compressible Liquid-Vapor Flow in Porous Media," *SIAM Journal on Mathematical Analysis*, vol. 52, no. 6, pp. 6155–6179, 2020.

[9] S. Metzger and P. Knabner, "Homogenization of two-phase flow in porous media from pore to Darcy scale: a phase-field approach," *Multiscale Modeling & Simulation. A SIAM Interdisciplinary Journal*, vol. 19, no. 1, pp. 320–343, 2021.

[10] Ľ. Baňas and H. S. Mahato, "Homogenization of evolutionary Stokes-Cahn-Hilliard equations for two-phase porous media flow," *Asymptotic Analysis*, vol. 105, no. 1-2, pp. 77–95, 2017.

[11] S. Sharmin, M. Bastidas, C. Bringedal, and I. S. Pop, "Upscaling of a Navier-Stokes-Cahn-Hilliard model for two-phase porous-media flow with solute-dependent surface-tension effects," in preparation.

[12] M. Bastidas, C. Bringedal, and I. S. Pop, "A two-scale iterative scheme for a phase-field model for precipitation and dissolution in porous media," *Applied Mathematics and Computation*, vol. 396, p. 125933, 2021.

[13] M. K. Brun, T. Wick, I. Berre, J. M. Nordbotten, and F. A. Radu, "An iterative staggered scheme for phase field brittle fracture propagation with stabilizing parameters," *Computer Methods in Applied Mechanics and Engineering*, vol. 361, p. 112752, 2020.

[14] M. Bastidas, C. Bringedal, I. S. Pop, and F. A. Radu, "Numerical homogenization of nonlinear parabolic problems on adaptive meshes," *Journal of Computational Physics*, vol. 425, p. 109903, 2020.